J. Cent. South Univ. (2020) 27: 592−607
DOI: https://doi.org/10.1007/s11771-020-4319-9

Springer

Effects of axial static stress on stress wave propagation in rock considering porosity compaction and damage evolution

JIN Jie-fang(金解放)[1], YUAN Wei(袁伟)[1], WU Yue(吴越)[2], GUO Zhong-qun(郭钟群)[1]

1. School of Architectural and Surveying Engineering, Jiangxi University of Science and Technology, Ganzhou 341000, China;
2. School of Resource and Environment Engineering, Jiangxi University of Science and Technology, Ganzhou 341000, China

Abstract: A wave equation of rock under axial static stress is established using the equivalent medium method by modifying the Kelvin-Voigt model. The analytical formulas of longitudinal velocity, space and time attenuation coefficients and response frequency are obtained by solving the equation using the harmonic method. A series of experiments on stress wave propagation through rock under different axial static stresses have been conducted. The proposed models of stress wave propagation are then verified by comparing experimental results with theoretical solutions. Based on the verified theoretical models, the influences of axial static stress on longitudinal velocity, space and time attenuation coefficients and response frequency are investigated by detailed parametric studies. The results show that the proposed theoretical models can be used to effectively investigate the effects of axial static stress on the stress wave propagation in rock. The axial static stress influences stress wave propagation characteristics of porous rock by varying the level of rock porosity and damage. Moreover, the initial porosity, initial elastic modulus of the rock voids and skeleton, viscous coefficient and vibration frequency have significant effects on the P-wave velocity, attenuation characteristics and response frequency of the stress wave in porous rock under axial static stress.

Key words: stress wave propagation; axial static stress; porosity compaction; space and time attenuation; response frequency

Cite this article as: JIN Jie-fang, YUAN Wei, WU Yue, GUO Zhong-qun. Effects of axial static stress on stress wave propagation in rock considering porosity compaction and damage evolution [J]. Journal of Central South University, 2020, 27(2): 592−607. DOI: https://doi.org/10.1007/s11771-020-4319-9.

1 Introduction

Rocks are natural geological materials consisting of solid minerals and pore space. The initial porosity and damage induced by external forces often govern the static and dynamic mechanical behaviors of rock [1−4]. The surrounding rocks in deep rock engineering have already been subjected to static stresses when a stress wave due to an earthquake or man-made blasting propagates through them. The magnitudes of the static stresses are variable because of the complexities of in situ stress field and the excavation unloading response of deep underground engineering. The porosity and damage degree of rock will change with the variation of the static stress, the full deformation of rock under uniaxial

Foundation item: Projects(51664017, 51964015) supported by the National Natural Science Foundation of China; Project(JXUSTQJBJ2017007) supported by the Program of Qingjiang Excellent Young Talents of Jiangxi University of Science and Technology, China; Projects(GJJ160616, GJJ171490) supported by Science and Technology Project of Jiangxi Provincial Department of Education, China
Received date: 2019-05-21; **Accepted date:** 2019-09-16
Corresponding author: JIN Jie-fang, PhD, Professor; Tel: +86-13576663880; E-mail: jjf_chang@126.com; ORCID: 0000-0001-9078-2728

compression includes the compaction or closure stage of initial microcracks, linear elastic stage, evolution stage of damage and post-peak stage [5−9], that is, the wave impedance of rock is deeply influenced by the axial static stress because of the stress−sensitivity relationships of longitudinal velocity and density [10]. Therefore, it is of importance to investigate the effects of static stress on stress wave propagation through rock.

Some experimental efforts have focused on the effects of stress on the wave velocity of rock [11−13]; in general, the wave velocity of rock increases during the compaction process and decreases during the damage phase with increasing stresses, and there are two empirical relationship expressions between stress and velocity: quadratic function and power function. The sensitivity of the rock wave velocity to static stress can be attributed to the closure of initial pores and the initiation and expansion of microcracks.

Based on the methods of the basic elements, such as Hooke body, Newton body and plastic body, Kelvin model, Maxwell model, generalized Maxwell model, Boltzmann model, Burger's model and modified model have been widely used in many filed of rock mechanics [4, 14, 15]. However, the above models fail to characterize non-linear rock deformation characteristics at the compaction stage of initial void. To overcome the deficiencies and limitations, CAO et al [16] presented a statistical damage constitutive model by considering the characteristics of the void compaction stage. Also, a cracked porous medium using the double-porosity model has been widely described and proved to be valid to describe the wave propagation [17−19].

The equivalent medium method (EMM) and displacement discontinuity method (DDM) are the two typical theoretical approaches to study wave propagation in rock and rock mass [20−23]. The EMM regards the porous rock and jointed rock mass as a continuous medium. Some attenuation and dissipation properties of stress wave in rock or rock mass have been achieved by combing the methods of EMM and element models. NIU et al [24] simulated the strain wave propagation in a artificial rock bar based on the Kelvin model, and developed an approach for determination of the viscosity coefficient of rock. Based on Boltzmann model, which consists of an auxiliary spring in series with a Kelvin model, FAN et al [25], LI et al [20], and WANG et al [26] established equivalent viscoelastic medium models for rock masses with different joint conditions, respectively. However, few studies have considered the propagation characteristics of the stress wave throughout the full deformation process of intact rock under static stress, especially during the compaction stage of initial void. There is no non-linear propagation model of stress wave for porous rock subjected to uniaxial compression.

The purpose of the paper is to focus on the effects of axial static stress on wave propagation through intact rock. A non-linear equivalent propagation model of stress wave through rock under full uniaxial compression deformation is established by improving the Kelvin model, which can quantify the influence of both compaction degree of initial microcrack and damage degree induced by axial static stress on the attenuation and dissipation of stress wave. Experiments of stress wave propagation in a long, red sandstone specimen under uniaxial compression are conducted to verify the analytical model. The effects of axial static stress on the wave velocity, the space and time attenuation characteristics of the wave amplitude and the response frequency are investigated.

2 Model establishment

2.1 Elements constitution of new model

Numerous experimental investigations have proved that there is a distinct closure stage of initial void and damage evolution stage when rock is under uniaxial compression, and the two stages account for the vast majority of a stress−strain curve. In addition, the stage of initial void compaction exhibits highly non-linear characteristics. Consequently, the selected elements in theoretical model should be able to represent the non-linear properties of the closure of initial void and damage evolution of rock. However, the previous models have failed to consider the effect of initial pore compaction of rock on attenuation and dissipation rules of stress wave, that is, there is no account of initial void of rock.

To remedy these shortages and investigate the effects of axial static stress on stress wave propagation of rock, the Kelvin model was improved by adding a new element of void body which was used to characterize the effect of the

initial void in rock on mechanical property, as shown in Figure 1. The rock skeleton is in series with the rock void firstly, then as a whole in parallel to the viscous body. It is noteworthy that the purpose of Ref. [16] is to describe the static mechanical property of rock, while our work is to explore the stress wave propagation in a rock. The rate-related effect of rock is remarkable while subjected to dynamic loading. And this phenomenon is mainly caused by the viscosity of rock. Therefore, to describe the pores compaction and viscosity of rock simultaneously, the improved model proposed in this paper includes three important elements of rock void body, rock skeleton body and viscous body. The rock void, rock skeleton and viscous body in Figure 1 are used to characterize the effects of initial void and its deformation, damage evolution deformation, and viscous property of rock under uniaxial compression on stress wave propagation, respectively. The means of both constructing initial voids and considering the effect of the deformation of initial void on stress wave propagation along porous rock are the innovations in this paper.

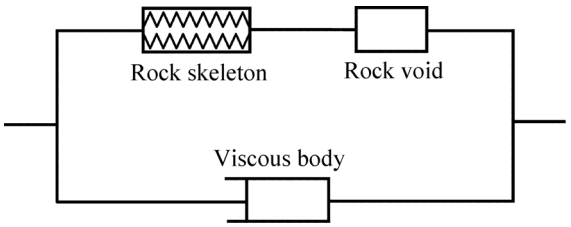

Figure 1 Schematic view of improved Kelvin model

2.2 Establishment of the wave equation

Because of the constitution relationship of rock skeleton, rock initial void and viscous body, shown in Figure 1, the stress and strain exhibit the following relationships, respectively:

$$\sigma = \sigma_{\mathbf{D}} + \sigma_\eta = (\sigma_s + \sigma_d) + \sigma_\eta \tag{1}$$

$$\varepsilon = \varepsilon_D = \varepsilon_\eta \tag{2}$$

where σ_D and ε_D are the stress and strain of the rock skeleton and void, respectively; σ_η and ε_η are the stress and strain of the viscous body, respectively; σ_s is the initial axial static stress; and σ_d is the dynamic stress due to the stress wave.

According to the characteristics of a viscous body, the viscous stress σ_η is directly proportional to the strain rate, and its constitutive equation can be expressed mathematically as:

$$\sigma_\eta = \eta \frac{\partial \varepsilon}{\partial t} \tag{3}$$

where the constant η is the viscous coefficient of a Newtonian body.

Based on the constitutive model of a void body [16], the constitutive equation of voids under coupled static and dynamic stresses, shown in Figure 1, can be expressed mathematically as:

$$\varepsilon_D^v = 1 - \exp\left(-\frac{\sigma_D}{E_1}\right) = 1 - \exp\left(-\frac{\sigma_s + \sigma_d}{E_1}\right) \tag{4}$$

where ε_D^v is the strain of the voids; σ_D is the axial stress of voids and consists of static stress σ_s and dynamic stress σ_d; and E_1 is the initial elastic modulus of voids.

The deformation of the rock skeleton part includes both elastic deformation and inelastic deformation. When the actual stress borne by rock skeletons is more than its yield strength, damage will occur in the rock skeleton. Combining the strain equivalence hypothesis of damage mechanics and generalized Hook's law, the strain of rock skeleton can be expressed mathematically as:

$$\varepsilon_D^r = \frac{\sigma_D}{E_2(1-D)} = \frac{\sigma_s + \sigma_d}{E_2(1-D)} \tag{5}$$

where ε_D^r is the strain of the rock skeletons; E_2 is the initial elastic modulus of the rock skeletons; D is the damage value of the rock under static stress coupled with stress wave-induced dynamic stress.

If the initial porosity of the damage body, shown in Figure 1, is γ_0, the corresponding proportion of rock skeletons in the damage body is $1-\gamma_0$, and the constitutive equation can be obtained from Eqs. (4) and (5) [16]:

$$\varepsilon_D = (1-\gamma_0)\frac{\sigma_s + \sigma_d}{E_2(1-D)} + \gamma_0\left(1 - \exp\left(-\frac{\sigma_s + \sigma_d}{E_1}\right)\right) \tag{6}$$

By taking the derivative with respect to x, Eq. (1) can be transformed into:

$$\frac{\partial \sigma}{\partial x} = \frac{\partial \sigma_d}{\partial x} + \frac{\partial \sigma_\eta}{\partial x} \tag{7}$$

Similarly, the derivative of Eq. (3) with respect to x is:

$$\frac{\partial \sigma_\eta}{\partial x} = \eta \frac{\partial^2 \varepsilon}{\partial t \partial x} \tag{8}$$

And the derivative of Eq. (6) with respect to x is:

$$\frac{\partial \varepsilon_{\mathrm{D}}}{\partial x}=\frac{1-\gamma_0}{E_2(1-D)}\frac{\partial \sigma_{\mathrm{d}}}{\partial x}+\frac{\gamma_0}{E_1}\exp\left(-\frac{\sigma_{\mathrm{s}}+\sigma_{\mathrm{d}}}{E_1}\right)\frac{\partial \sigma_{\mathrm{d}}}{\partial x} \tag{9}$$

Simplifying the form of Eq. (9) can obtain:

$$\frac{\partial \sigma_{\mathrm{d}}}{\partial x}=\frac{1}{\beta}\frac{\partial \varepsilon_D}{\partial x} \tag{10}$$

where $\beta=\frac{1-\gamma_0}{E_2(1-D)}+\frac{\gamma_0}{E_1}\exp\left(-\frac{\sigma_{\mathrm{s}}+\sigma_{\mathrm{d}}}{E_1}\right)$, which is the reciprocal of equivalent modulus of stressed porous rock. The axial static stress σ_{s} and dynamic stress σ_{d} play key roles in the parameter β, in addition to the void proportion γ_0 and initial elastic moduli E_1 and E_2. If there is no initial void, that is, γ_0=0, then $\beta=\frac{1-\gamma_0}{E_2(1-D)}+\frac{\gamma_0}{E_1}\exp\left(-\frac{\sigma_{\mathrm{s}}+\sigma_{\mathrm{d}}}{E_1}\right)=\frac{1}{E_2(1-D)}$, which is the reciprocal of the modulus of the damage body.

Substituting Eqs. (8) and (10) into Eq. (7) yields:

$$\frac{\partial \sigma}{\partial x}=\frac{1}{\beta}\frac{\partial \varepsilon}{\partial x}+\eta\frac{\partial^2 \varepsilon}{\partial t\partial x} \tag{11}$$

According to the motion equation of the stress wave, $\rho\frac{\partial v}{\partial t}=\frac{\partial \sigma}{\partial x}$, Eq. (11) can be transformed into:

$$\rho\frac{\partial^2 u}{\partial t^2}=\frac{1}{\beta}\frac{\partial^2 u}{\partial x^2}+\eta\frac{\partial^3 u}{\partial x^2\partial t} \tag{12}$$

where ρ is the density of porous rock; u is the particle vibration displacement.

Eq. (12) is the wave equation of porous rock considering the effects of both the initial voids and axial static stress. Based on the expression of the equivalent elastic parameter β, if there are no initial voids in rock, Eq. (12) will evolve into a conventional wave equation of rock.

2.3 Solutions to wave equation

This paper focuses on investigating the effects of initial stress and initial voids on the propagation attenuation characteristics of rock. The harmonic method of solving the wave equation can characterize the amplitude, frequency and wave number of wave compared with the traveling wave method. Supposing that the distance between a vibrating particle and the seismic source is x, the harmonic equation can be expressed as [27]:

$$u(x,t)=u_0\mathrm{e}^{i(\omega_1 t-k_{\mathrm{t}}x)} \tag{13}$$

where u_0, ω_1 and k_{t} are the amplitude, angular frequency and wave number of the harmonic wave, respectively.

Substituting Eq. (13) into Eq. (12) yields:

$$\rho\omega_1^2=\frac{1}{\beta}k_{\mathrm{t}}^2+\eta k_{\mathrm{t}}^2\omega_1 i \tag{14}$$

Because Eq. (14) involves complex numbers, the angular frequency ω_1 should be a complex number when wave number k_{t} is a real number, and it is assumed that its form can be defined as follows:

$$\omega_1=\omega_w+\alpha_{\mathrm{t}}i \tag{15}$$

where ω_w is the response frequency, and α_{t} is the time attenuation coefficient.

Substituting Eq. (15) into Eq. (14) yields:

$$\rho\left(\omega_w^2-\alpha_{\mathrm{t}}^2\right)+2\rho\omega_w\alpha_{\mathrm{t}}i=\eta k_{\mathrm{t}}^2\omega_w i-\eta k_{\mathrm{t}}^2\alpha_{\mathrm{t}}+\frac{k_{\mathrm{t}}^2}{\beta} \tag{16}$$

From Eq. (16), the complex numbers on the left and right sides must have the equal real and imaginary components, so the following equations can be obtained:

$$\alpha_{\mathrm{t}}=\frac{\eta k_{\mathrm{t}}^2}{2\rho} \tag{17}$$

$$\omega_w^2=\frac{k_{\mathrm{t}}^2}{\rho\beta}-\frac{\eta^2 k_{\mathrm{t}}^4}{4\rho^2} \tag{18}$$

With increases in the propagation distance, the stress wave inevitably decays; the direct results of the decay are the amplitude attenuation and energy dissipation. To investigate the attenuation characteristics of the wave with respect to the propagation distance, the harmonic wave form is rewritten as [27]:

$$u(x,t)=u_0\mathrm{e}^{-\alpha_{\mathrm{s}}x}\mathrm{e}^{i\left(\omega_q t-k_{\mathrm{s}}x\right)} \tag{19}$$

where α_{s} is the spatial attenuation coefficient; ω_q is the vibration frequency; k_{s} is the spatial response wave number.

Substituting Eq. (19) in Eq. (12) yields:

$$\rho\omega_q^2=\frac{k_{\mathrm{s}}^2-\alpha_{\mathrm{s}}^2}{\beta}+2\eta k_{\mathrm{s}}\alpha_{\mathrm{s}}\omega_q+\left[\eta\left(k_{\mathrm{s}}^2\omega_q-\alpha_{\mathrm{s}}^2\omega_q\right)-\frac{2k_{\mathrm{s}}\alpha_{\mathrm{s}}}{\beta}\right]i \tag{20}$$

According to the condition that the left side is equal to the right side in Eq. (20), the following

equations can be derived:

$$\eta\left(k_{\mathrm{s}}^2\omega_q-\alpha_{\mathrm{s}}^2\omega_q\right)=\frac{2k_{\mathrm{s}}\alpha_{\mathrm{s}}}{\beta} \tag{21}$$

$$\rho\omega_q^2=\frac{k_{\mathrm{s}}^2-\alpha_{\mathrm{s}}^2}{\beta}+2\eta k_{\mathrm{s}}\alpha_{\mathrm{s}}\omega_q \tag{22}$$

The specific expressions of spatial response wave number k_{s} and spatial attenuation coefficient α_{s} can be obtained by solving Eqs. (21) and (22) as follows:

$$k_{\mathrm{s}}^2=\frac{\rho\omega_q^2\beta\left(\sqrt{1+\beta^2\omega_q^2\eta^2}+1\right)}{2\left(1+\eta^2\omega_q^2\beta^2\right)} \tag{23}$$

$$\alpha_{\mathrm{s}}^2=\frac{\rho\omega_q^2\beta\left(\sqrt{1+\beta^2\omega_q^2\eta^2}-1\right)}{2\left(1+\eta^2\omega_q^2\beta^2\right)} \tag{24}$$

Based on the relations among the wave number, wave velocity and frequency, the P-wave velocity under different frequencies C_q can be calculated by Eq. (23):

$$C_q^2=\frac{\omega_q^2}{k_{\mathrm{s}}^2}=\frac{2\left(1+\eta^2\omega_q^2\beta^2\right)}{\rho\beta\left(\sqrt{1+\beta^2\omega_q^2\eta^2}+1\right)} \tag{25}$$

Assuming that k_t=k_{s}, the attenuation coefficient with respect to time α_{t} and the response frequency of rock ω_w can be obtained by substituting Eq. (23) into Eqs. (17) and (18), respectively:

$$\alpha_{\mathrm{t}}=\frac{\omega_q^2\beta\eta\left(\sqrt{1+\beta^2\omega_q^2\eta^2}+1\right)}{4\left(1+\eta^2\omega_q^2\beta^2\right)} \tag{26}$$

$$\omega_w^2=\frac{\rho\omega_q^2\beta\left(\sqrt{1+\beta^2\omega_q^2\eta^2}+1\right)}{2\left(1+\eta^2\omega_q^2\beta^2\right)}\times\left(\frac{1}{\rho\beta}-\frac{\omega_q^2\eta^2\beta\left(\sqrt{1+\beta^2\omega_q^2\eta^2}+1\right)}{8\rho\left(1+\eta^2\omega_q^2\beta^2\right)}\right) \tag{27}$$

Eqs. (24)−(27) are the stress wave propagation models for porous rock under axial static stress. Based on the stress wave propagation models, the effects of the initial porosity γ_0, the axial static stress σ_{s}, the dynamic stress σ_{d}, the initial modulus E_1 and E_2, the viscous coefficient η, and the vibration frequency ω_q on stress wave space attenuation coefficient α_{s}, time attenuation coefficient α_{t}, propagation velocity C_q, and response frequency ω_w may be investigated when the models are verified to be correct and feasible.

3 Verification of theoretical results

To evaluate the feasibility and validity of the theoretical analysis, a series of experiments on stress wave propagation through rock under different axial static stresses have been conducted.

3.1 Rock specimens and experimental devices

The rock specimens were prepared by red sandstone. Their dimensions of the rock specimens are 80 mm×80 mm×1500 mm, and the incident and transmitted ends were ground by a grinding machine to satisfy the flatness and end parallelism requirement. Strain waves of the different propagation distances in rock specimen were measured by 5 pairs of strain gauges, which are shown in Figure 2, labeled for A, B, C, D and E, respectively. In order to minimize the influence of eccentric compression on measured data when stress wave propagation in rock specimen, the 5 pairs of strain gauges in Figure 2 were glued on the upper and lower lateral surfaces of rock specimen, respectively, distributing along their longitudinal symmetric axes; in addition, each pair of strain gauges were attached symmetrically across a same cross-section of the specimen.

The physical and mechanical parameters of red sandstone are shown in Table 1, where E_1 and E_2

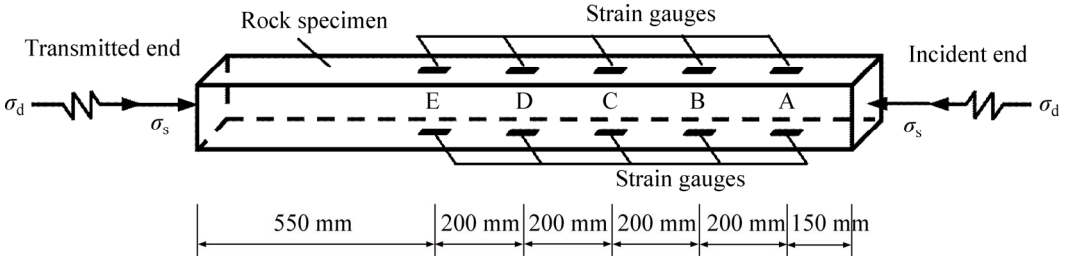

Figure 2 Dimensions of the rock specimens and locations of the strain gauges (σ_{s} and σ_{d} denote the axial static stress and dynamic stress, respectively)

denote the initial elastic modulus of the voids and the skeletons of red sandstone, respectively; the symbols of ρ, C, γ_0 and η denote the density, longitudinal wave velocity, porosity and viscosity coefficient of red sandstone, respectively. It is noted that the porosity of the rock specimen in Table 1 was measured using the method of nuclear magnetic resonance. Based on stress−strain curves of red sandstone under uniaxial compression, the values of E_1 and E_2 were obtained by using the determining method of E_1 and E_2 [16]. According to the experimental data of stress wave propagation along red sandstone under the elastic deformation of uniaxial compression, the viscosity coefficient η was determined using the determining method of viscosity coefficient [24].

The laboratory testing setup used here is a modified split Hopkinson pressure bar (SHPB), as shown in Figure 3, which can furnish axial static loading separately apart from impact loading [28].

Table 1 Physical and mechanical parameters of red sandstone

ρ/(kg·m^{-3})	C/(m·s^{-1})	E_1/MPa	E_2/GPa	γ_0	η/(MPa·s)
2406	2260	31.9	3.26	0.0538	9.5

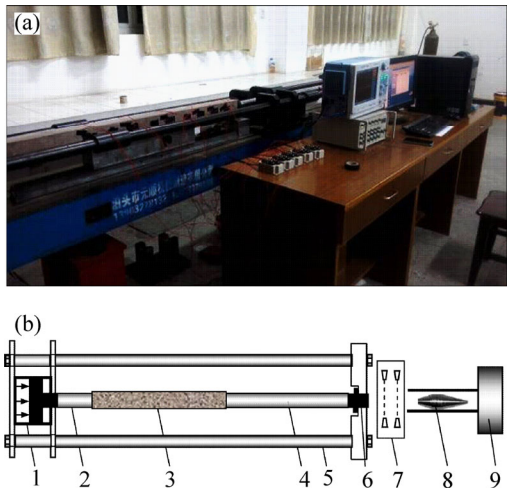

Figure 3 Photograph of experimental apparatus: (a) Schematic view of the experimental method; (b) Schematic view of experimental method (1−Axial pre-compression stress inducer; 2−Transmission bar; 3−Rock specimen; 4−Incident bar; 5−Frame; 6−Thin baffle screen; 7−Laser velocimeter; 8−Special-shape striker; 9−Gas tank)

The components of the modified SHPB used in the present study are made up of an axial pre-compression stress inducer, a striking system, an incident bar, a transmission bar and a data acquisition system. The diameter of both the incident bar and transmitted bar is 50 mm. The data acquisition unit comprises a SDY2017A ultrahigh dynamic strainometer, a DL850E oscilloscope and a desktop computer. The rock specimen with all strain gauges attached to the respective locations was sandwiched between the incident bar and transmission bar coaxially.

Because the cross-sectional areas of the incident and transmission bars are smaller than that of the rock specimen, two stainless steel disks with areas larger than that of the specimen were sandwiched between the incident bar, specimen and transmitted bar in series to eliminate the non-uniform compression of the specimen. The impact between the special-shaped striker and the thin baffle screen, shown in Figure 3, generates a compression strain wave propagating from incident bar to rock specimen. The strain wave amplitude can be adjusted by changing the impact velocity of the striker, and the striking velocities were measured with a JXCS-02 laser velocimeter.

3.2 Experimental purpose and method

Experiments were performed in this study to verify the proposed theoretical models. The experimental spatial amplitude attenuation coefficients, stress wave velocities and main frequencies of rock under different axial static stresses were chosen for comparison with the theoretical results, which were obtained by substituting the parameter values in Table 1 into Eqs. (24), (25) and (27).

In line with the stress wave propagation process of the modified SHPB, the stress wave travels into the rock specimen through the incident bar and is measured with the corresponding location gauges. To investigate the effect of axial static stress on stress wave propagation and minimize the influence of the stress wave on damage to the rock, the impact velocities of the striker are kept a constant of 4.38 m/s. The axial pre-stresses of rock in the experiments are classified into 13 groups: 0, 2.76, ⋯, 33.13 MPa, with an interval of 2.76 MPa.

3.3 Experimental results

Figure 4 only shows the strain waves of the rock specimens under 5 axial static stress conditions; the other strain wave results are omitted in this

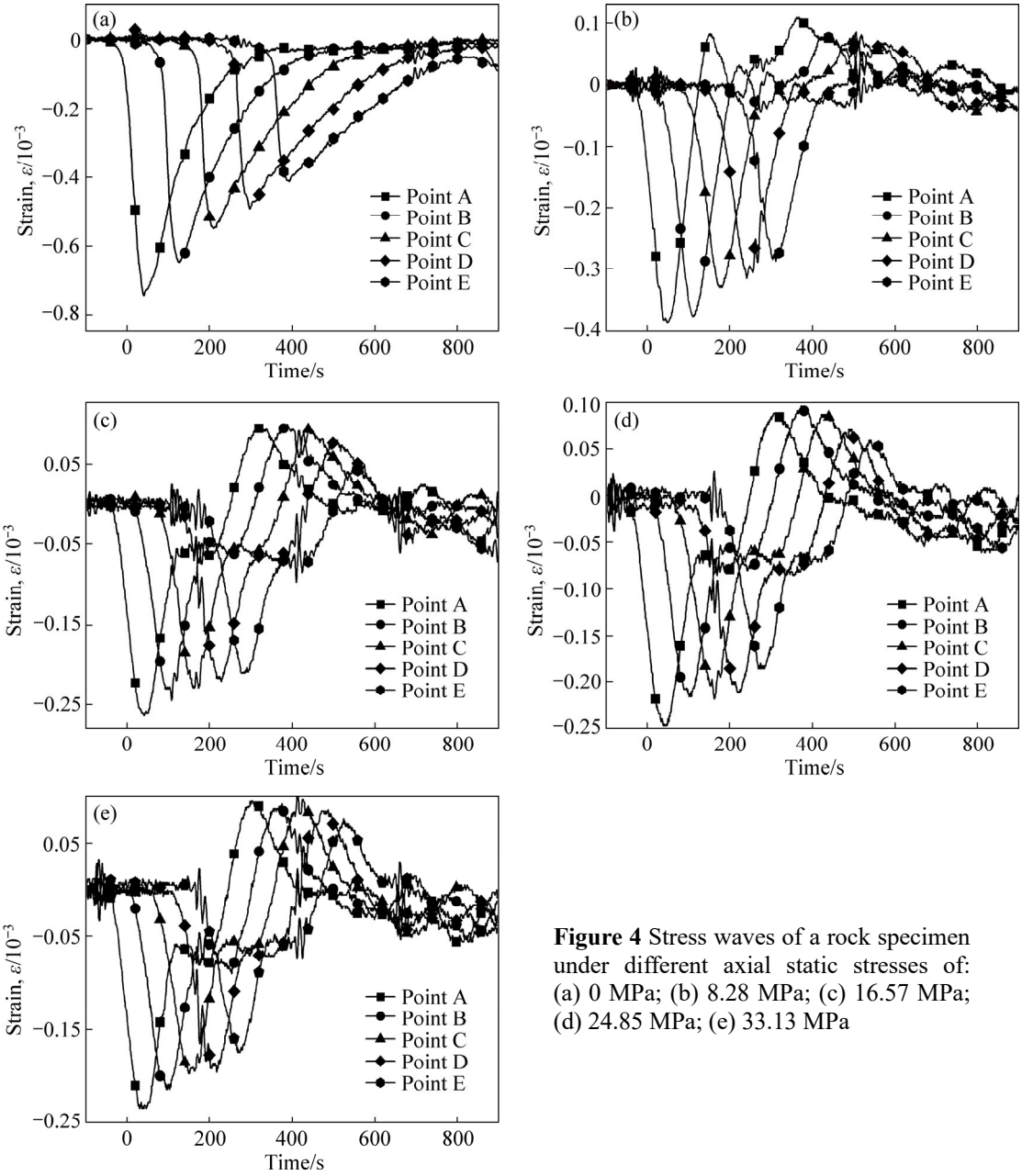

Figure 4 Stress waves of a rock specimen under different axial static stresses of: (a) 0 MPa; (b) 8.28 MPa; (c) 16.57 MPa; (d) 24.85 MPa; (e) 33.13 MPa

paper due to space limitations. It is evident that the amplitude of strain wave decreases gradually with the increase in propagation distance when the axial static stress is determined, but their waveforms are similar. The axial pre-stress has a significant effect on the stress wave, the amplitude of the stress wave at a given point decreases with increasing static stress, and the tensile wave appearing at the tail of the stress wave will increase with increasing axial static stress.

All the key experimental parameters are listed in Table 2, where ε_A denotes the absolute value of stress wave amplitude and t is the time corresponding to the amplitude.

3.4 Comparisons between experimental and theoretical results

To facilitate the analysis, Figure 5 shows the frequency spectra (0−10000 Hz) of point A under different axial static stresses based on the results of the fast Fourier transform (FFT) to the stress wave signals in Figure 4. Figure 5 shows that the experimental stress waves are not single-frequency signals, and their frequency bands range from approximately 0 to 3000 Hz. In addition, the principal frequencies approach to 1400 Hz with increasing axial static stress; therefore, the vibration frequency ω_q in the subsequent analytical calculation is fixed to 1400 Hz.

Table 2 Experimental results

Axial static stress/MPa	Point A		Point B		Point C		Point D		Point E		Striking velocity/ (m·s^{-1})
	$\varepsilon_A/10^{-3}$	t/μs	$\varepsilon_A/10^{-3}$	t/μs	$\varepsilon_A/10^{-3}$	t/μs	$\varepsilon_A/10^{-3}$	t/μs	$\varepsilon_A/10^{-3}$	t/μs	
0.00	0.7453	142	0.6480	227	0.5507	311	0.4920	398	0.4133	494	4.316
2.76	0.6173	155	0.5613	218	0.4800	299	0.4293	372	0.3600	452	4.482
5.52	0.4987	152	0.4693	214	0.4147	289	0.3773	356	0.3320	429	4.472
8.28	0.3867	148	0.3760	210	0.3293	276	0.3147	341	0.2867	413	4.488
11.04	0.3227	141	0.3160	212	0.2840	266	0.2720	334	0.2573	398	4.427
13.81	0.2907	142	0.2773	202	0.2533	266	0.2467	323	0.2373	393	4.398
16.57	0.2640	142	0.2453	209	0.2293	261	0.2213	330	0.2107	378	4.302
19.33	0.2613	142	0.2307	201	0.2213	257	0.2187	327	0.2093	378	4.406
22.09	0.2520	137	0.2280	199	0.2267	259	0.2173	314	0.1987	374	4.325
24.85	0.2467	140	0.2160	202	0.2187	263	0.2120	322	0.1853	372	4.335
27.61	0.2444	149	0.2213	192	0.2080	252	0.2040	316	0.1920	379	4.402
30.37	0.2373	149	0.2200	204	0.2080	261	0.1920	318	0.1840	382	4.294
33.13	0.2347	131	0.2147	197	0.1973	250	0.1960	319	0.1747	380	4.283

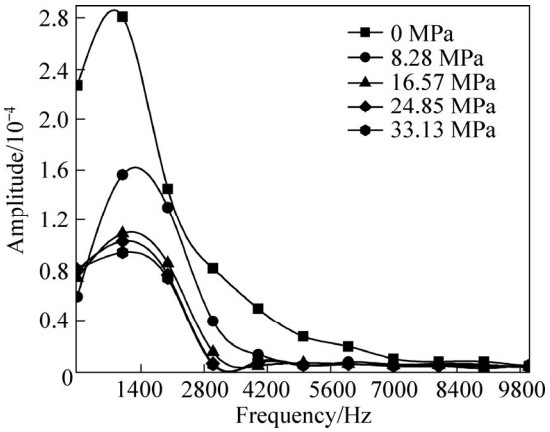

Figure 5 Frequency spectra of point A under different static stresses

The distance Δl between points A and E along the rock specimen, shown in Figure 2, is 800 mm, and the time difference between the stress wave onset times of points A and E shown in Figure 4 is the wave propagating time Δt. The propagation velocity $\bar{C}$ of stress wave, which is the longitudinal wave velocity or P-wave velocity, can be calculated by:

$$\bar{C} = \Delta l / \Delta t \tag{28}$$

The corresponding theoretical P-wave velocities of rock under different axial stresses can be obtained on the basis of Eq. (25), where ω_q=1400 Hz; σ_d=17.5 MPa, being determined by the dynamic peak stress of point A when the axial static stress is zero; and the other parameter values shown in Table 1.

Figure 6 shows the comparison between the experimental data and theoretical results by the proposed analytical solution. The variation tendency of the wave velocities calculated by the proposed method corresponds well with the experimental data, verifying that the above analytical solutions are feasible and reasonable.

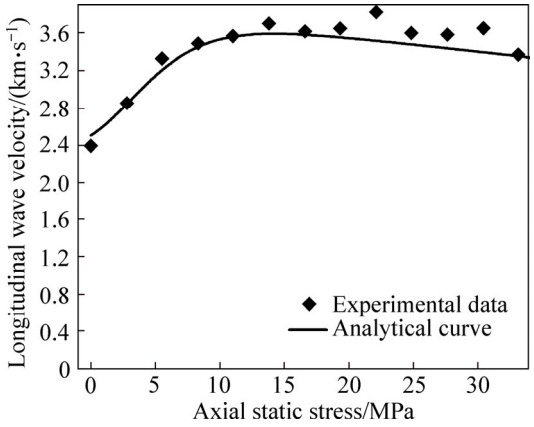

Figure 6 Relationship of P-wave velocity vs. axial static stress

Based on the experimental results of the strain waves shown in Table 2, the spatial attenuation property of a stress wave can be investigated based on the wave amplitudes with respect to different points or propagation distances. The relationship between wave amplitudes and propagation distances under specific axial static stresses can be fitted with a linear function, where the slope of the fitting line denotes the amplitude attenuation along

the propagation distance and is referred to as the spatial attenuation coefficient in this paper.

Based on Eq. (24) and the parameter values in Table 1, and vibration frequencies of ω_q=900, 1400, 1800 and 2800 Hz, the theoretical values of the rock spatial attenuation coefficient can be obtained. Figure 7 shows the experimental and analytical spatial attenuation coefficients of rock with different vibration frequency values.

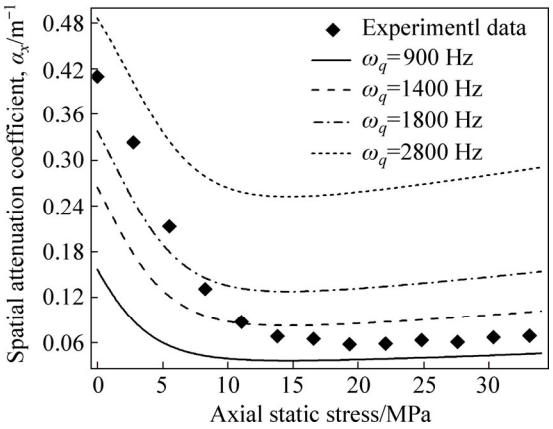

Figure 7 Spatial attenuation coefficients of experimental data and analytical data with ω_q=900, 1400, 1800 and 2800 Hz under different axial static stresses

Figure 7 reveals that the trends of the theoretical spatial attenuation coefficients correspond well with the experimental results with the increase in axial static stress. However, Figure 7 also reveals that there are large deviations between the theoretical and experimental coefficients; the theoretical results are lower than the experimental data when the vibration frequency is small, and the spatial attenuation coefficients obtained by the theoretical method increase with increasing vibration frequency until they exceed the experimental results. The possible reasons for the deviations are as follows: the proposed theoretical solutions are obtained by solving the wave equation based on the harmonic method, which means that the frequency in the theoretical solution is a single frequency. In contrast, the frequency components in the experimental signals are relatively complex, as can be seen from the frequency spectrum shown in Figure 5. The values of vibration frequency ω_q used in Figure 7 are in the range of main frequencies, and close to the principal frequency, it is conceivable that the deviations in Figure 7 will decrease if the bandwidths of the experimental signals narrow gradually. Therefore, Figure 7 proves that the present theoretical solution can effectively describe the effect of axial static stress on the spatial attenuation properties of the stress wave.

The principal frequencies obtained by FFT to all strain waveforms in Figure 4 are referred as the response frequencies ω_w, and the vibration frequency ω_q is fixed to 1400 Hz. The experimental values of ω_w/ω_q under different axial static stresses are shown in Figure 8.

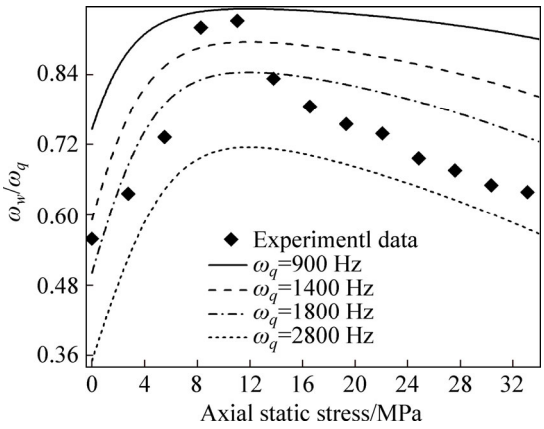

Figure 8 ω_w/ω_q of experimental data and analytical data with ω_q=900, 1400, 1800 and 2800 Hz under different axial static stresses

Based on Eq. (27) and vibration frequencies of ω_q=900, 1400, 1800 and 2800 Hz, with the values of the other parameters being identical to those in Figure 6, the analytical values of ω_w/ω_q under different axial static stresses are shown in Figure 8. Figure 8 shows that the same variation trend occurs in the experimental and analytical results with increase in axial static stress, and the analytical values with different vibration frequencies deviate from the corresponding experimental results. For the same reason with Figure 7, the complex frequency components of the experimental signal vs. the single frequency of the analytical solution may be the essential reason, which gives rise to the deviations between the analytical and experimental data in Figure 8. Therefore, the comparisons in Figure 8 verify the feasibility of the theoretical solution.

4 Effects of axial static stress on stress wave propagation

In this section, parametric studies are conducted to investigate the influences of axial

static stress on the stress wave propagation via the longitudinal wave velocity, space and time attenuation coefficient, and response frequency. The influences of the initial elastic modulus of voids E_1, initial elastic modulus of rock skeletons E_2, initial porosity γ_0, viscous coefficient of rock η, and vibration frequency ω_q in Eqs. (23)−(27) are also included in the analysis. To simplify the analysis, the damage evolution of rock under axial static pressure is assumed to be proportional to the axial static stress σ_s, i.e., $D(\sigma_s)=K\sigma_s$, where K is the slope, and the damage D=1 when σ_s is equal to the uniaxial compressive strength.

4.1 Variations in longitudinal velocity

Based on Eq. (25), the relationships between the longitudinal wave velocity and axial static stress are shown in Figure 9 considering the influences of different parameters. The basic parameter values in Figure 9 are shown in Table 3.

Figure 9 shows that the longitudinal wave velocity initially increases but then decreases with increasing axial static stress. This phenomenon occurs because as the axial static stress increases, the closure of initial micro-crack of rock occurs firstly, and then damage emerges because of the initiation, propagation and coalescence of cracks.

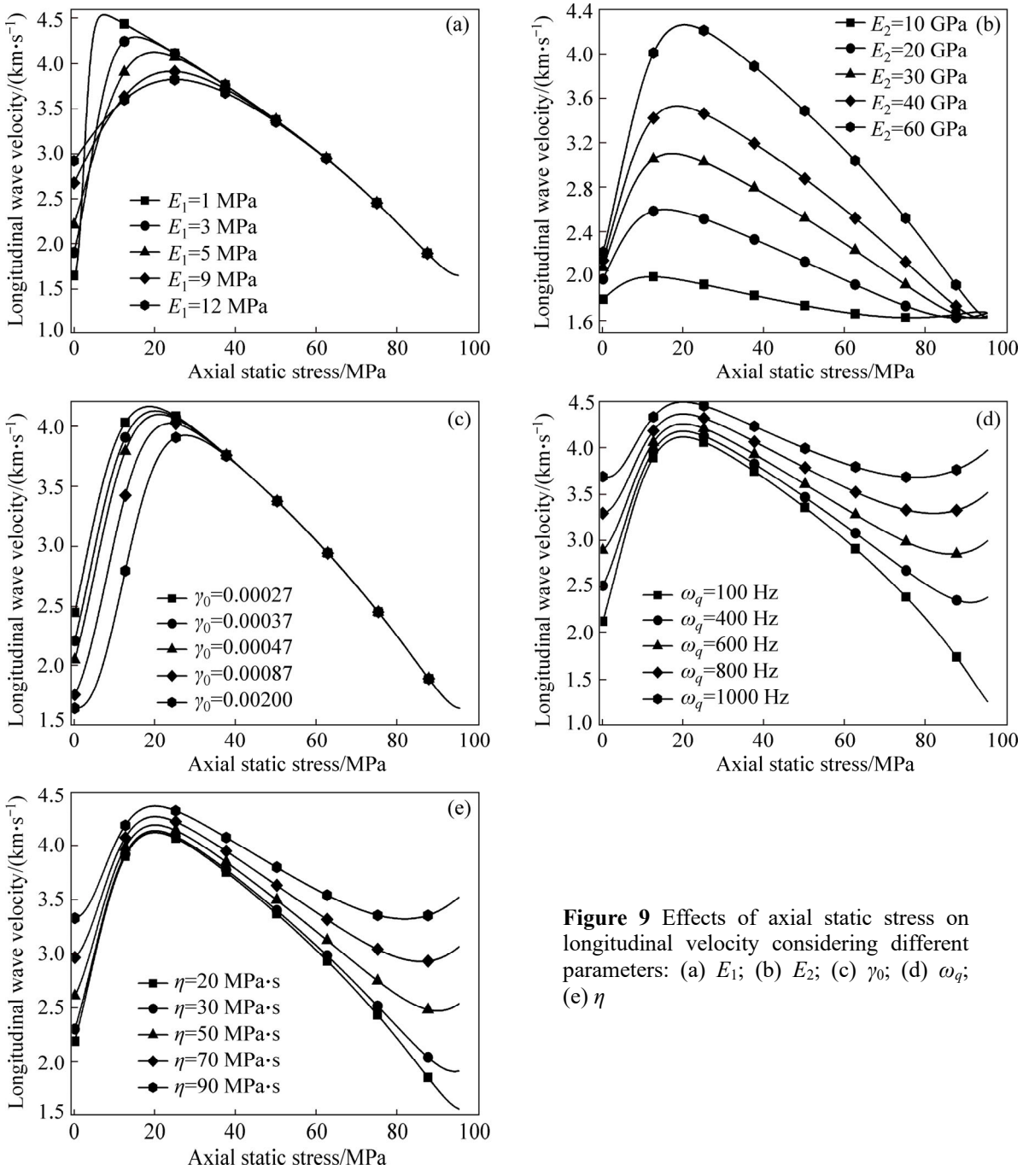

Figure 9 Effects of axial static stress on longitudinal velocity considering different parameters: (a) E_1; (b) E_2; (c) γ_0; (d) ω_q; (e) η

Table 3 Basic parameter values in Figure 9

Figure No.	σ_d/ kPa	E_1/ MPa	E_2/ GPa	γ_0	ω_q/ Hz	η/ (MPa·s)
9(a)	5	1 3 5 9 12	56	0.00037	200	22
9(b)	5	5	10 20 30 40 60	0.00037	200	22
9(c)	5	5	56	0.00027 0.00037 0.00047 0.00087 0.00200	200	22
9(d)	5	5	56	0.00037	100 400 600 800 1000	22
9(e)	5	5	56	0.00037	200	20 30 50 70 90

The density and modulus of the rock initially increase and then decrease with the deformation process. The variation trends are in good agreement with the other experimental studies [11, 12, 13], which verifies the analytic solutions to some extent.

Figure 9 also reveals that many parameters have important effects on the longitudinal wave velocity of rock under axial stress. Figure 9(a) shows that when axial static stress is comparatively small, the little increase in the initial elastic modulus of voids gives rise to a huge variation in P-wave velocity. On the contrary, when the axial static stress is sufficiently large, the effect of parameter E_1 becomes minimal or nearly zero. Between the two regions, the effect law of parameter E_1 is contrary to that in the small stress region. In contrast, the influence law of the initial elastic modulus of rock skeletons is comparatively simple, as shown in Figure 9(b); a larger modulus E_2 results in a greater longitudinal wave velocity during the axial loading process, which coincides with classical elastic wave theory. Figure 9(c) shows that in the small axial stress region, an increase in the initial porosity γ_0 results in a decrease in the P-wave velocity, and the effect of the initial porosity γ_0 becomes zero when the axial stress is sufficiently large. Similarly, the vibration frequency ω_q exerts a considerable influence on the P-wave velocity of rock under uniaxial compression deformation, as shown in Figure 9(d), and there is a continuous increase in the longitudinal wave velocity with increases in the frequency ω_q. The relations between the effective velocity and incident wave frequency for in situ stressed rock mass also have similar results [20]. Figure 9(e) shows that the P-wave velocity of rock increases with increasing viscosity coefficient η.

4.2 Space and time attenuation coefficients

Based on Eq. (24), the relationships between the spatial attenuation coefficient and axial static stress are shown in Figure 10. Considering the influences of different parameters, the parameter values in Figure 10 are identical to those in Figure 9.

Based on Eq. (26), the relationships between the time attenuation coefficient and axial static stress are shown in Figure 11. The parameter values in Figure 11 are same with those in Figure 9.

Figures 10 and 11 show that both the spatial attenuation coefficient α_s and time attenuation coefficient α_t initially decrease rapidly, then develop gently, and ultimately increase rapidly with increasing axial static stress. These phenomena are attributed to the density variation and damage evolution of porous rock under uniaxial compression deformation, the deformation of rock under uniaxial compression includes four stages of initial void compaction, transient elastic deformation, crack initiation and propagation and post peak failure, and the corresponding porosity or damage degree of rock under decreases initially, then remains unchanged almost, subsequently increases rapidly with increasing axial static stress. Consequently, the above variation rules of space and time attenuation coefficients along with increasing axial static stress occur, where a larger rock porosity or damage degree is associated with

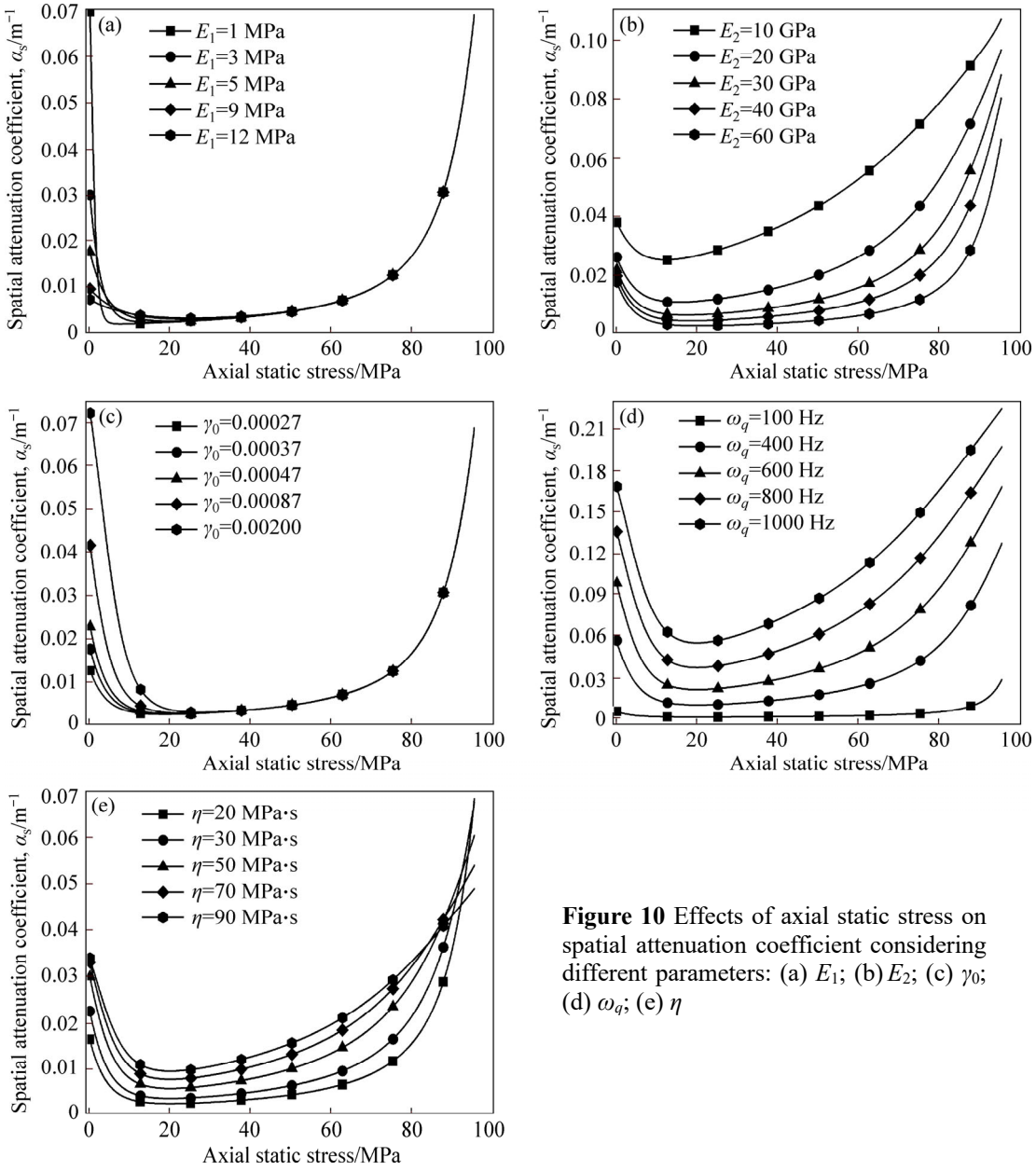

Figure 10 Effects of axial static stress on spatial attenuation coefficient considering different parameters: (a) E_1; (b) E_2; (c) γ_0; (d) ω_q; (e) η

larger energy dissipations with respect to traveling distance and time.

Figure 10 shows that the spatial attenuation coefficient α_s is dependent on the parameters E_1, E_2, γ_0, ω_q, and η. Figure 10(a) indicates that the initial modulus of voids E_1 has a significant influence on the spatial attenuation coefficient when the axial static stress is less than 20 MPa, whereas the influence gradually approaches zero with increasing axial static stress. For example, the spatial attenuation coefficient decreases with increases in the parameter E_1 when the axial stress is equal to zero, which is contrary to the relation between the P-wave velocity and parameter E_1. Figure 10(b) shows that the spatial attenuation coefficients with different initial moduli E_2 are different for certain axial stresses, and a larger parameter E_2 is associated with a smaller coefficient α_s. Figure 10(c) shows that the influence of the initial porosity γ_0 on parameter α_s is rather significant when axial stress is less than 20 MPa, where a larger initial porosity γ_0 results in a larger attenuation coefficient α_s, which corresponds to the experimental results showing that the energy dissipation ratio increases with increasing porosity. Meanwhile, the influence weakens with increasing axial static stress. Figure 10(d) shows that for any given axial stress, the spatial attenuation coefficient increases with increasing vibration frequency ω_q, and the jointed rock mass and damaged rock have

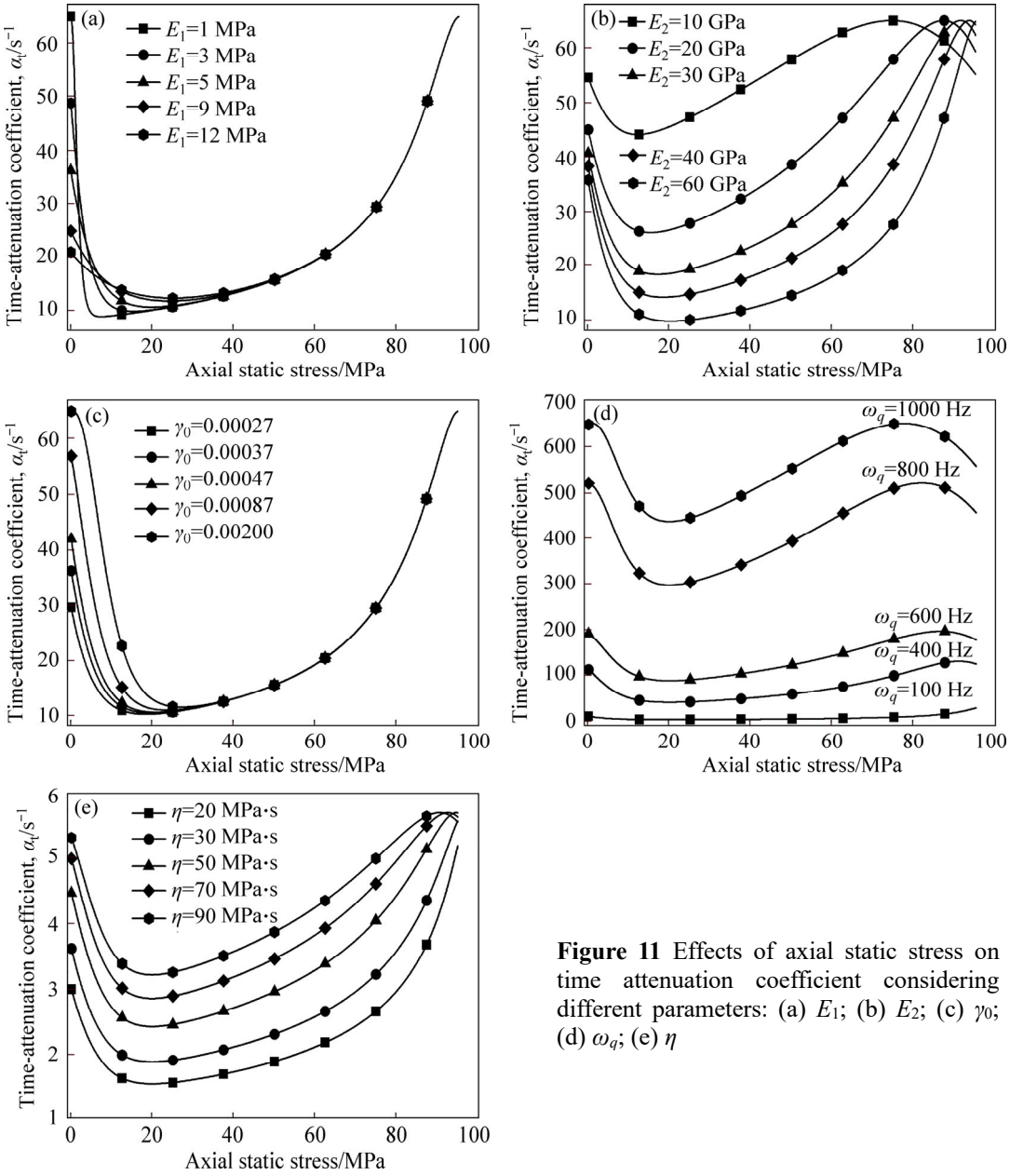

Figure 11 Effects of axial static stress on time attenuation coefficient considering different parameters: (a) E_1; (b) E_2; (c) γ_0; (d) ω_q; (e) η

similar relationships between attenuation and incident frequency [20, 29]. The results indicate that the high frequency stress wave is more likely to attenuate than the low-frequency wave when propagating through rock under any axial stress. Figure 10(e) shows that with a fixed axial stress, the viscosity coefficient η of deformed rock likewise influences the spatial attenuation properties of stress wave propagation; a larger parameter η results in a larger coefficient α_s.

A comparison of Figures 10 and 11 shows that the effects of the parameters E_1, E_2, γ_0, ω_q and η on the time attenuation coefficient α_s of rock are consistent with the effects on the spatial attenuation coefficient α_t.

4.3 Variations in response frequency

In this section, the ratio ω_w/ω_q is used to characterize the variations in the response frequency of porous rock under uniaxial compression. Figure 12 shows the ratio ω_w/ω_q of rock under different axial static stresses considering the influences of different parameters, and the parameter values in Figure 12 are identical to those in Figure 9.

Figure 12 illustrates that the axial static stress has a considerable effect on the stress wave response frequency of rock throughout the uniaxial compression deformation process; with increasing axial stress, the ratio of ω_w/ω_q initially increases rapidly, then increases gradually, and ultimately

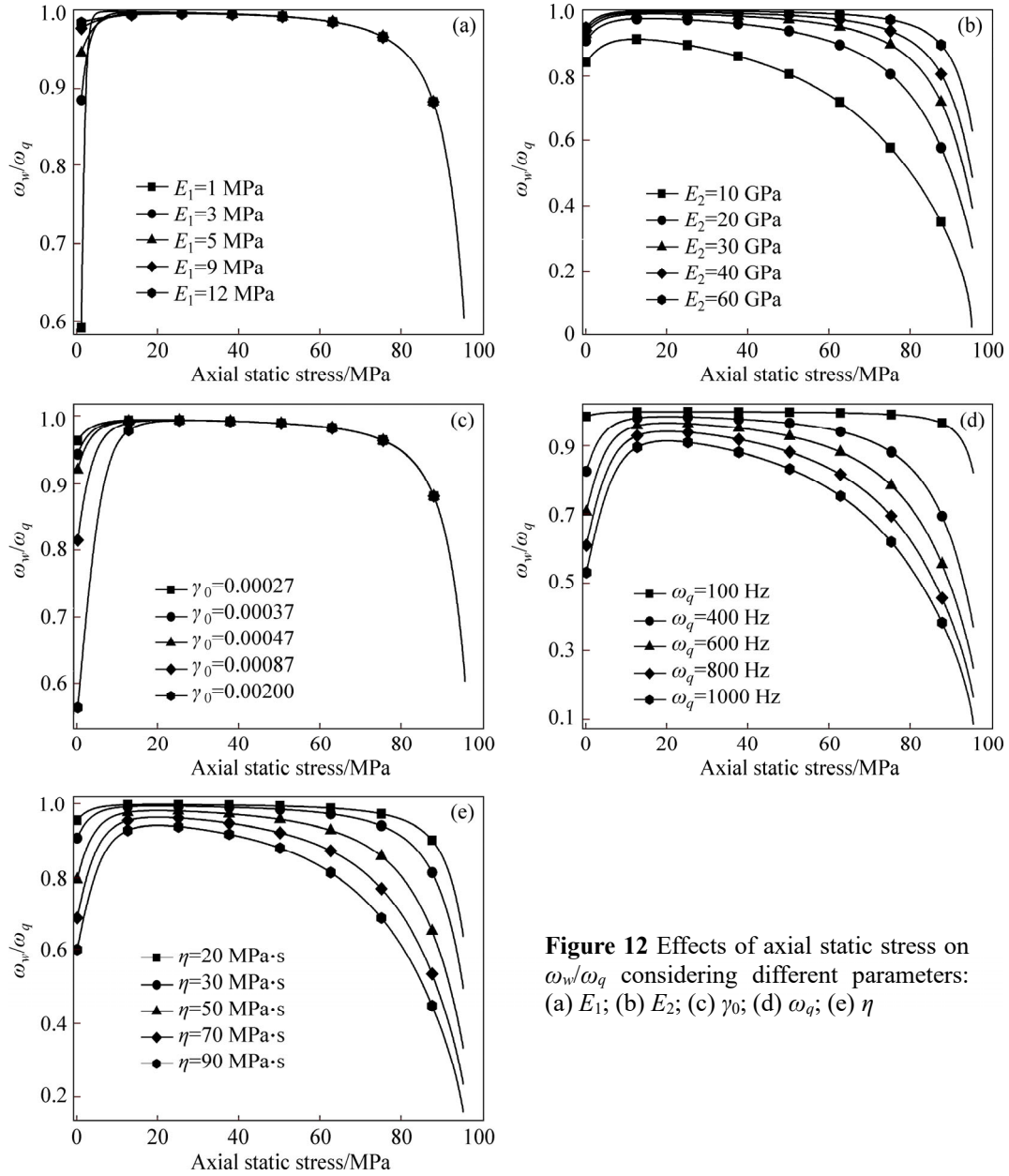

Figure 12 Effects of axial static stress on ω_w/ω_q considering different parameters: (a) E_1; (b) E_2; (c) γ_0; (d) ω_q; (e) η

decreases rapidly.

Figure 12 also shows that the response frequency ω_w is influenced by the parameters E_1, E_2, γ_0, ω_q, and η. As shown in Figure 12(a), the parameter E_1 affects the response frequency ω_w considerably when static stress equals zero, and the influence gradually weakens with increasing axial static stress. In contrast, Figure 12(b) shows that the initial modulus E_2 of the rock skeleton has a persistent effect on the response frequency of rock throughout the axial loading process. For any given static stress, a larger parameter E_2 results in a larger ratio of ω_w/ω_q. Similarly, the initial porosity γ_0 influences the frequency ω_w when the static stress is small; a larger porosity signifies a smaller frequency ω_w, which means that the larger porosity of rock results in a more rapid attenuation of the frequency wave. In addition, based on Figure 12(d), the response frequency ω_w is affected by the vibration frequency ω_q as well; a larger frequency ω_q produces a smaller ratio of ω_w/ω_q of rock under any axial static stress. A comparison of Figures 12(d) and (e) shows that the influence laws of the viscosity coefficient η on response frequency is similar to that of the vibration frequency.

5 Conclusions

This study proposes a viscoelastic equivalent medium model to investigate the effects of static

stress and different physical and mechanical parameters on the stress wave propagation of porous rock. Experiments on stress wave propagation through long red sandstone specimens with different axial static stresses are conducted using a modified SHPB device. The effects of axial stress on the longitudinal wave velocity, space and time attenuation coefficients and response frequency of rock are investigated through parametric studies. The influences of the initial porosity, initial moduli of the voids and skeleton, vibration frequency and viscosity coefficient are discussed. The main conclusions are as follows:

1) The proposed theoretical model is effective and feasible for investigating the effects of axial static stress on the stress wave propagation through rock during the uniaxial compression deformation process.

2) The porosity and damage of a rock influence propagation characteristics of stress wave by changing the effective elastic modulus of the rock.

3) Because of the porosity variation and damage evolution induced by axial static stress, with increasing axial stress, the longitudinal wave velocity and response frequency initially increase but then decrease. In contrast, the space and time attenuation coefficients initially decrease and then increase. Overall, the variation trends are significant in the low and high axial stress regions, while the variations are gentle between these two extreme stress regions.

4) During the uniaxial compression deformation process of porous rock, the characteristics of stress wave propagation are influenced by the initial modulus, initial porosity, viscosity coefficient, of the rock and the frequency of stress wave.

List of symbols

E_1, E_2	Initial elastic modulus of the voids and the rock skeletons
ε_D, ε_η	Strains of the damage and viscous body
ε_D^v, ε_D^r	Strains of voids and the rock skeletons
σ_D, σ_η	Stresses of the damage and viscous body
σ_s, σ_d	Axial initial static stress, and dynamic stress
γ_0	Initial porosity of porous rock
η	Viscous coefficient of a Newton body
x	Propagation distance
t	Time
β	Equivalent parameter of the effective modulus for porous rock
ω_q, ω_w	Vibration and response frequencies of rock
k_t, k_s	Time and space wave number
α_t, α_s	Time and space attenuation coefficient
C_q, $\overline{C}$	Theoretical and experimental P-wave velocity
ε_A	Absolute value of stress wave amplitude

References

[1] HEIDARI M, KHANLARI G R, TORABI-KAVEH M, KARGARIAN S, SANEIE S. Effect of porosity on rock brittleness [J]. Rock Mech Rock Eng, 2014, 47: 785−790. DOI: 10.1007/s00603-013-0400-0.

[2] PATRICK B, WONG T F, ZHU W. Effects of porosity and crack density on the compressive strength of rocks [J]. Int J Rock Mech Min Sci, 2014, 67: 202−211. DOI: 10.1016/ j.ijrmms. 2013.08.031.

[3] HAN De-hua, NUR A, MORGAN D. Effects of porosity and clay content on wave velocities in sandstones [J]. Geophysics, 1986, 51: 2093−2107. DOI: 10.1190/1.1442062.

[4] HOU Rong-bin, ZHANG Kai, TAO Jing, XUE Xin-ran, CHEN Yan-long. A nonlinear creep damage coupled model for rock considering the effect of initial damage [J]. Rock Mech Rock Eng, 2019, 52: 1275−1285. DOI: 10.1007/ s00603-018-1626-7.

[5] MENG Qing-bin, ZHANG Ming-wei, HAN Li-jun, PU Hai, CHEN Yan-long. Acoustic emission characteristics of red sandstone specimens under uniaxial cyclic loading and unloading compression [J]. Rock Mech Rock Eng, 2018, 51(4): 969−988. DOI: 10.1007/s00603-017-1389-6.

[6] MUNOZ H, TAHERI A, CHANDA E K. Pre-peakand post-peak rock strain characteristics during uniaxial compression by 3D digital image correlation [J]. Rock Mech Rock Eng, 2016, 49(7): 2541−2554. DOI: 10.1007/s00603-016-0935-y.

[7] LI Yan-rong, HUANG Da, LI Xi-an. Strain rate dependency of coarse crystal marble under uniaxial compression: strength, deformation and strain energy [J]. Rock Mech Rock Eng, 2014, 47(4): 1153−1164. DOI: 10.1007/s00603-013-0472-x.

[8] FENG Xia-ting, CHEN Si-li, ZHOU Hui. Real-time computerized tomography (CT) experiments on sandstone damage evolution during triaxial compression with chemical corrosion [J]. Int J Rock Mech Min Sci, 2004, 41(2): 181−192. DOI:10.1016/S1365-1609(03)00059-5.

[9] WONG Teng-fong, BAUD P. The brittle-ductile transition in porous rock: A review [J]. J Struct Geol, 2012, 44: 25−53. DOI: 10. 1016 /j. jsg. 2012. 07. 010.

[10] JIN Jie-fang, LI Xi-bing, YIN Zhi-qiang, ZOU Yang. A method for defining rock damage variable by wave

impedance under cyclic impact loadings [J]. Rock and Soil Mechanics, 2011, 32(5): 1385−1393,1410. DOI:10.1631/jzus. B1000185.

[11] SUN Qiang, ZHU Shu-yun. Wave velocity and stress/strain in rock brittle failure [J]. Environ Earth Sci, 2014, 72(3): 861−866. DOI: 10. 1007 /s12665 -013-3009-4.

[12] CHEN Xiang, SUN Jin-zhong, TAN Chao-shuang, ZHANG Jie-kun, XU Zhao-yi. Relation between P-wave velocity and stress of rock samples and their unloading effect [J]. Chin J Rock Mech Eng, 2010, 32: 757−761. http://manu31.magtech. com.cn/Jwk_ytgcxb/ CN/.

[13] FREUND D. Ultrasonic compressional and shear velocities in dry clastic rocks as a function of porosity, clay content, and confining pressure [J]. Geophys J Int, 1992, 108(1): 125−135. DOI: 10.1111/j.1365-246X.1992.tb00843.x.

[14] MOGILEVSKAYA S G, LECAMPION B. A lined hole in a viscoelastic rock under biaxial far-field stress [J]. Int J Rock Mech Min, 2018, 106: 350−363. DOI: 10.1016/j.ijrmms. 2018.02.019.

[15] ZHANG Jian-zhi, ZHOU Xiao-ping, YIN Peng. Visco-plastic deformation analysis of rock tunnels based on fractional derivatives [J]. Tunn Undergr Space Technol, 2019, 85: 209−219. DOI: 10.1016/j.tust.2018.12.019.

[16] CAO Wen-gui, ZHANG Chao, HE Min, LIU Tao. Statistical damage simulation method of strain softening deformation process for rocks considering characteristics of void compaction stage [J]. Chin J Rock Mech Eng, 2016, 38: 1754−1761. DOI: 10.11779/CJGE201610002.

[17] BERRYMAN, JAMES G. Long wavelength propagation in composite elastic media II. Ellipsoidal inclusions [J]. J Acoust Soc Am, 1980, 68(6): 1820−1831. DOI: 10.1121/ 1.385172.

[18] CAO Cheng-hao, FU Li-yun, BA Jing, ZHANG Yan. Frequency-and incident-angle-dependent P-wave properties influenced by dynamic stress intera-ctions in fractured porous media [J]. Geophysics, 2019, 84(5): 1−53. DOI: 10.1190/geo2018- 0103.1.

[19] ZHANG Lin, BA Jing, CARCIONE J M, SUN Wei-tao. Modeling wave propagation in cracked porous media with penny-shaped inclusions [J]. Geophysics, 2019, 84(4): 1−38. DOI: 10.1190/GEO2018-0487.1.

[20] LI J C, LI H B, ZHAO J. An improved equivalent viscoelastic medium method for wave propagation across layered rock masses [J]. Int J Rock Mech Min Sci, 2015,73: 62−69. DOI:10.1016/j.ijrmms.2014.10.008.

[21] FAN L F, SUN H Y. Seismic wave propagation through an in-situ stressed rock mass [J]. J Appl Geophys, 2015, 121: 13−20. DOI: 10.1016 /j. jappgeo. 2015.07.002.

[22] ZHAO J, ZHAO X B, CAI J G. A further study of P-wave attenuation across parallel fractures with linear deformational behaviour [J]. Int J Rock Mech Min Sci, 2006, 43(5): 776−788. DOI: 10.1016/j.ijrmms. 2005.12.007.

[23] LI J C, LI H B, MA G W, ZHAO J. A time-domain recursive method to analyse transient wave propagation across rock joints [J]. Geophys J Int, 2012, 188(2): 631−644. DOI: 10.1111/j.1365-246X.2011.05286.x.

[24] NIU Lei-lei, ZHU Wang-cheng, LI Shao-hua, GUAN Kai. Dete-rmining the viscosity coefficient for viscoelastic wave propagation in rock bars [J]. Rock Mech Rock Eng, 2018, 51(5): 1347−1359. DOI: 10.1007/s00603-018-1407-3.

[25] FAN L F, MA G W, LI J C. Nonlinear viscoelastic medium equivalence for stress wave propagation in a jointed rock mass [J]. Int J Rock Mech Min Sci, 2012, 50: 11−18. DOI: 10.1016/j.ijrmms.2011.12.008.

[26] WANG Rui, HU Zhi-ping, ZHANG Dan, WANG Qi-yao. Propagation of the stress wave through the filled joint with linear viscoelastic deformation behavior using time-domain recursive method [J]. Rock Mech Rock Eng, 2017, 50(12): 3197−3207. DOI: 10.1007/s00603-017-1301-4.

[27] WANG Li-li. Foundations of stress waves [M]. Amsterdam: Elsevier, 2007. DOI: 10.1016/B978-008044494-9/50014-7.

[28] LI Xi-bing B, ZHOU Zi-long, LOK T S, HONG Liang, YIN Tu-bing. Innovative testing technique of rock subjected to coupled static and dynamic loads [J]. Int J Rock Mech Min Sci, 2008, 45(5): 739−748. DOI:10.1016/j.ijrmms.2007. 08.013.

[29] LIU Cang-li, AHRENS T J. Stress wave attenuation in shock-damaged rock [J]. J Geophys Res, 1997, 102(B3): 5243−5250. DOI: 10.1029/ 96jb03891.

(Edited by ZHENG Yu-tong)

中文导读

考虑空隙压密及损伤演化的轴向静应力对岩石应力波传播的影响研究

摘要：本文基于等效介质方法，通过改进 Kelvin-Voigt 模型，建立了具有轴向静应力空隙岩石的波动方程。利用谐波法求解波动方程，得到了用纵波波速、时空衰减系数和响应频率等表征的应力波传播理论模型。选用红砂岩制备岩石试件，进行了室内具有轴向静应力岩石的应力波传播试验。通过对比试验和理论模型结果，验证了应力波传播模型的正确性。基于应力波传播理论模型，通过参数研究方法探讨了轴向静应力对岩石应力波波速、时空衰减系数和响应频率的影响。结果表明，本文提出的应力波传播理论可以有效表征轴向静应力对岩石应力波传播的影响，轴向静应力通过改变岩石的有效孔隙度和损伤度影响岩石的应力波传播特性。初始空隙度、岩石空隙和骨架的初始模量、黏性系数和振动频率对岩石应力波波速、衰减系数以及响应频率等都有较大的影响。

关键词：应力波传播；轴向静应力；空隙压密；时空衰减；响应频率